Direct Numerical Simulation of a Paradigmatic Urban Heat Island

Pavan, Anna; Costa, Pedro; Stalio, Enrico; Cimarelli, Andrea

DOI
10.18280/ijht.430506

Publication date
2025

Document Version
Final published version

Published in
International Journal of Heat and Technology

Citation (APA)
Pavan, A., Costa, P., Stalio, E., & Cimarelli, A. (2025). Direct Numerical Simulation of a Paradigmatic Urban Heat Island. *International Journal of Heat and Technology*, *43*(5), 1679-1685. https://doi.org/10.18280/ijht.430506

International Journal of Heat and Technology
Vol. 43, No. 5, October, 2025, pp. 1679-1685
Journal homepage: http://iieta.org/journals/ijht

Direct Numerical Simulation of a Paradigmatic Urban Heat Island

Anna Pavan[1*], Pedro Costa[2], Enrico Stalio[1], Andrea Cimarelli[1]

[1] Department of Engineering "Enzo Ferrari", University of Modena and Reggio Emilia, Modena 41125, Italy
[2] Process & Energy Department, TU Delft, CB Delft 2628, The Netherlands

Corresponding Author Email: anna.pavan@unimore.it

https://doi.org/10.18280/ijht.430506

Received: 19 July 2025
Revised: 9 September 2025
Accepted: 17 September 2025
Available online: 31 October 2025

Keywords:
UHI, direct numerical simulation, turbulence, heat transfer

ABSTRACT

In the last decades the urban population has increased a lot making cities objects of different studies. In this context, urban climate is an expanding research field and understanding the main features of the urban heat island (UHI) effect is one of the challenges. A discrete number of neighbourhoods has been object of study for this climate effect with growing interest in recent years, especially focusing on heat mitigation. Despite this, there is a lack of knowledge due to the complex nature of the problem given by the multi-physics involved, the multiple parameters that govern it and above all, the complexity of the city's geometries that lack generality. In this respect, and to keep results applicable in a broader context, this work proposes an innovative approach to studying UHI effects, providing a unique framework for understanding the interaction between urban geometry and heat transport dynamics while addressing the complexities of urban configurations with a novel and methodological perspective.

1. INTRODUCTION

In recent decades, global population growth has accelerated, and various projections indicate that it will continue rising steadily in the coming years. As a result, urban areas are expected to expand significantly, given their high population density. Whitin this evolving urban context, cities are particularly vulnerable to meteorological hazards due to the concentration of people, assets, infrastructure, and capital stocks [1], which has led to growing concern over urban climate issues and contributed to the rapid expansion of this research field [2].

Among the most studied phenomena in urban climate is the Urban Heat Island (UHI). As the term implies, UHIs are urbanized areas that are warmer than their surroundings, with a wide range of consequences, from impacts on human health to ecological changes.

Urban systems are inherently complex, and the UHI effect is largely influenced by the artificialization of the surface [3]. Heat produced by human activities and absorbed from solar radiation during the day is mainly stored within urban canopy elements and subsequently released during night time, making cities warm even during the night hours.

For this reason, the UHI phenomenon can be classified into diurnal and nocturnal types and can also be categorized based on the geographical setting of the city, since the surrounding areas interact with the urban canopy.

From its early documentation in London [4], the UHI phenomenon has presented a variety of scientific challenges, as it differs across cities and is driven by multiple interacting factors. As such, it has attracted considerable attention from disciplines including climatology, environmental science, architecture, materials science, energy engineering, urban planning, and public health [5].

Several studies in literature have examined the UHI phenomenon in real urban environments such as Hannover (Germany) [6], Toulouse (France) [2], and city across South Asia, for a review see the study of Kotharkar et al. [7] as some examples.

These studies provide valuable insight into how UHI manifests in diverse geographic and climatic contexts.

One of the main drivers of UHI effect is the urban canopy, which lies within the Urban Canopy Layer (UCL), the atmospheric layer extending from the ground up to the height of the dominant urban elements.

Understanding the complex dynamic that occurs within UCL is essential for accurately representing cities in weather and climate models. Since the urban microclimate is shaped by a range of physical processes occurring within the canopy layer, reliable urban parametrizations are essential for improving the performance of weather forecasting models.

At the neighborhood scale ranging from few meters up to 1 kilometer, variations in building form and density significantly influence airflow, thereby affecting the transport of momentum, heat, and pollutants within the urban environment [8]. However, in mesoscale atmospheric models such as, weather research and forecasting WRF model, buildings are not explicitly resolved. Instead, urban areas are represented through simplified, parameterized surface characteristics.

Building morphology plays a key role in these parameterizations. Urban models often describe city structures using morphological parameters such as the plan area index, ratio between the total buildings area and the total plan area, the frontal area index, the ratio between the building frontal

area to the total plan area, and the average building height. Many parameterizations for airflow above cities are based on these and similar surface descriptors [1, 9-11].

Although few studies have attempted to simulate small portions of real urban, but simplified, environments, such as RANS simulations over parts of central London [12] on in Zhao old town [13], as in Basel [14], or wind tunnel experiments replicating selected districts [15, 16], most numerical investigations still adopt idealized geometries.

These configurations typically consist of simplified arrangements of cubic or rectangular blocks, either aligned or staggered, and often include elongated blocks to represent urban canyons. Such geometric simplifications are commonly used in both CFD simulations and wind tunnel experiments.

For instance, Xie and Castro [17] investigated flow over staggered wall-mounted cube of different heights using numerical simulations, Ricciardelli and Polimeno [18] explored airflow behavior in wind tunnels; and Zaki et al. [19] examined vertical wind profile within a canopy layer. Additional numerical studies of urban canopy flow on staggered and non-staggered cuboids are reported by Castro et al. [20].

Idealized configurations remain essential for identifying general flow behaviors and isolating the effects of key morphological parameters in urban environments.

Our study aligns with this line of research, aiming to develop a general understanding of the UHI phenomenon from a fluid dynamic perspective. To achieve this, we adopt a bottom-up approach, which aims to identify and analyze the fundamental physical processes governing urban atmospheric flows. This method emphasizes the role of key parameters, rather than relying on detailed reconstructions of specific urban configurations, which would constrain the applicability of the results to a narrow range of scenarios.

Since our analysis focuses on parameters related solely to urbanization, in our approach, the urban canopy is modelled as a rough surface composed of simplified hexahedral buildings arranged in a circular domain of radius R and not aligned with the computational grid. The urban layout is characterized by five key non-dimensional parameters: The average coverage frequency λ, the average density coverage ρ, the average aspect ratio of the planform area AR_π, and the average aspect ratio of the building heights AR_z along with ε, a coefficient describing the radial variation of the city shape. As it will be shown these parameters effectively capture the main statistical features of cities and enable a generalized modelling approach. To the authors' knowledge, this study presents the first investigation of the UHI under purely convective conditions, in the absence of external wind, within this paradigmatic setup using Direct Numerical Simulation.

The paper is organized as follows. Section 2 describes the algorithm employed to generate the idealized urban pattern. Section 3 outlines the numerical method and the governing equations. The flow topology and main statistics are described in Section 4, while Section 5 concludes the study with final remarks.

2. CITY PARAMETRIZATION

When considering an urban canopy into a climate model, it is not feasible to resolve the detailed geometry of individual buildings within each grid cell. Therefore, a geometrical approximation of the urban structure is required. As outlined in the previous section, one approach is to simplify the representation by considering an idealized city. In our approach, this simplification consists of representing the urban canopy as a rough surface composed of hexahedral buildings, distributed within a circular domain of radius R.

A key feature of this technique is that, by varying these five parameters, it is possible to generate an arbitrary number of distinct roughness configurations, or equivalently, distinct city patterns, while statistically preserving the overall characteristics across buildings and the urban layout.

As a result, each building exhibits unique dimensions, shape, and orientations, ensuring morphological diversity within a statistically consistent framework.

In our study, we identified a minimal set of five parameters to characterize any urban pattern. The first four parameters are:

$$\lambda = \frac{R}{\sqrt{A_\pi}} \tag{1}$$

$$\rho = \frac{nA_\pi}{\pi R^2} \tag{2}$$

$$AR_\pi = \frac{l_x}{l_y} \tag{3}$$

$$AR_z = \frac{l_z}{\sqrt{A_\pi}} \tag{4}$$

where, λ is the ratio between the city radius and the average building planform length, ρ the average density coverage, AR_π the average building planform aspect ratio and AR_z the average building vertical aspect ratio.

In the above relations, n denotes the total number of buildings, A_π is the average building planform area, l_z is the average building vertical length and l_x, l_y are the average shorter and longer building planform lengths respectively.

The fifth parameter is ε, which controls the variation of the urban canopy along the radial direction as defined by:

$$g(r) = \begin{cases} e^{-(x^2+y^2)/\varepsilon R^2}, & x^2+y^2 \le R^2 \\ 0, & x^2+y^2 > R^2 \end{cases} \tag{5}$$

$$AR_{zcity} = g(r)AR_z \tag{6}$$

with AR_{zcity} the average city vertical aspect ratio.

To compute the parameters, the city radius R must be set. As it defines the reference length, we assign it the value of 1. With all parameters defined, the pattern generation process proceeds in three main steps. First, the dimensions of each building are computed using Eqs. (7)-(9) and a specific orientation is assigned according to Eq. (10).

$$l_x = \sqrt{A_\pi AR_\pi f_{random}}, \qquad f_{random} \in [0.5; 1.5] \tag{7}$$

$$l_y = \frac{l_x}{AR_\pi} f'_{random}, \qquad f'_{random} \in [0.5; 1.5] \tag{8}$$

$$l_z = \sqrt{A_\pi} AR_z \, f''_{random}, \qquad f''_{random} \in [0.5; 1.5] \tag{9}$$

$$\gamma = \frac{\pi}{2} f'''_{random}, \qquad f'''_{random} \in [-0.5; 0.5] \tag{10}$$

$$x_2 = x_1 + l_{free} + l_x \tag{11}$$

$$l_{free} = l_{free}^{ref} f_{random}'''', f_{random}'''' \in [0.5; 1.5] \tag{12}$$

$$l_{free}^{ref} = \frac{R}{n} - \sqrt{A_\pi} \tag{13}$$

where, f_{random} are generator functions of random numbers that are used to brake symmetries in the city pattern as it is real world scenarios.

Then the square domain is populated with n buildings by applying the last three relations, Eqs. (11)-(13) along *x* and *y* axis (see Figure 1).

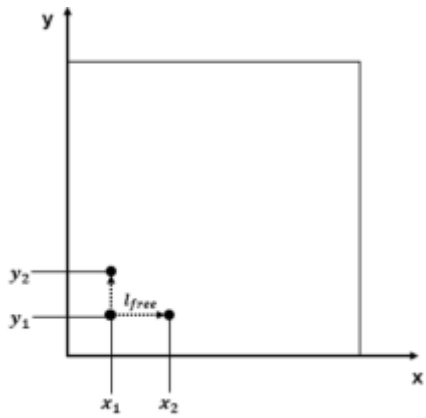

Figure 1. Starting domain

The final step of the procedure consists in smoothing the entire geometry using a truncated Gaussian distribution Eqs. (5) and (6), which ensure that all elements lie within a circular domain of radius R, centred on the initial domain. In this configuration, the tallest buildings are located at the city centre, while their height progressively decreases towards the edge.

For our simulation, the specific set of five parameters used to generate the urban configuration is reported in Table 1. The final configuration consists of 176 buildings (see Figure 2), located within the circular target area of radius $R = 1$.

Table 1. City parameters

λ	ρ	AR_π	AR_z	ε
20	0.8	1.5	1.5	1

Figure 2. Zoom-in of the created city pattern

3. EQUATIONS AND NUMERICAL METHOD

3.1 Equations

The flow is investigated within a slightly modified Rayleigh–Bénard Convection (RBC) setup. The governing equations are formulated under the Boussinesq approximation, in which density is assumed to be constant except for when it directly causes buoyant forces [21]. They are expressed in the following non dimensional form:

$$\frac{\partial u_i}{\partial x_i} = 0 \tag{14}$$

$$\frac{\partial u_i}{\partial t} + \frac{\partial u_i u_j}{\partial x_j} = -\frac{\partial p}{\partial x_i} + \sqrt{\frac{Pr}{Ra}} \frac{\partial^2 u_i}{\partial x_j \partial x_j} + \vartheta \delta_{i_3} \tag{15}$$

$$\frac{\partial \vartheta}{\partial t} + \frac{\partial \vartheta u_j}{\partial x_j} = \frac{1}{\sqrt{RaPr}} \frac{\partial^2 \vartheta}{\partial x_i \partial x_i} \tag{16}$$

The variables u_i , p, and ϑ denote the velocity, pressure, and the temperature fields respectively. The indices *i,j* =1, 2, 3, where $u_1 = u$, and $u_2 = v$ denotes the horizontal velocity components, $u_3 = w$ is the vertical component, and $\delta_{i,j}$ represents the Kronecker delta. The dimensionless form Eqs. (14)-(16) is obtained by using the cell height H, the temperature difference $\Delta\Theta$ between the maximum temperature within the city and the temperature of the top plate and the free-fall velocity $U_{ff} = \sqrt{g\beta\Delta\Theta H}$ as characteristic scales. The Prandtl number is given by the ratio between the kinematic viscosity υ and thermal diffusivity α, i.e., $Pr = \upsilon/\alpha$ while the Rayleigh number is given by $Ra = g\beta\Delta\Theta H^3/\nu\alpha$ where β is the thermal expansion coefficient and g is the gravitational acceleration.

3.2 Numerical method

The Direct Numerical Simulation of this idealized city pattern is performed using the open-source code CaNS [22]. Spatial discretization is based on a second order finite difference scheme on a staggered grid, while time integration is achieved by a three-step Runge-Kutta scheme with a Courant–Friedrichs–Lewy (CFL) condition of 0.6.

The simulation employs an immersed boundary method (IBM), specifically the formulation by Yang and Balaras [23], to handle the complex urban geometry. To this end, a signed distance field ϕ, (SDF) of the created geometry is provided as input to the solver with values defined at each grid point in the domain. This scalar field enables a representation of the solid boundaries: positive values of ϕ indicate fluid regions, negative values correspond to solid regions and the fluid–solid interface is defined by the iso-surface $\phi = 0$.

This representation is essential for identifying the forcing points, grid nodes closest to the immersed surface, as well as the interpolation points, used to reconstruct the velocity field at those locations. In IBM approaches, an additional force term is added into the right-hand side of the Navier-Stokes equation to enforce the desired velocity boundary condition at the immersed surface. In our case, the IBM consists of four main steps. The first two are executed only once at the beginning of the simulation, since the boundaries are stationary. In this initialization phase, the solver determines the forcing points, defined above. Then, for each forcing point, it determines three interpolation points, which are later used to reconstruct the velocity field at those locations.

The remaining steps are performed at each time step. Hence, the velocity field is interpolated at the previously identified interpolation points, and the corresponding forcing term is computed and applied to the forcing points to enforce the desired boundary condition at the fluid-solid interface.

This simulation is performed for a fixed Prandtl number *Pr* = 0.7, corresponding to air, and for Rayleigh number, $Ra = 10^8$. The computational domain is a rectangular box of

size $(Lx, Ly, Lz) = (8,8,1.05)$, where x, y are the horizontal axes and z is the wall normal vertical coordinate. It is worth noting that the reference length used for non-dimensionalization is $H = 1$, corresponding to vertical distance between the ground surface, at the base of the buildings and the top plate.

The domain is discretized using $(nx, ny, nz) = (1600,1600,263)$ set grid points. In the vertical direction, a hyperbolic tangent stretching is applied to ensure the correct resolution near the walls.

Boundary conditions for the velocity field are defined as follows: periodic boundary conditions are applied at the lateral directions, while no-slip boundary condition is used at the bottom plate and free-slip boundary condition is set at the top plate. A schematic representation of the domain can be seen in Figure 3.

Regarding the temperature field, an isothermal condition is imposed at the top plate, with $\vartheta_{cold} = -0.5$, while lateral sides are treated as periodic. At the bottom plate, a non-uniform temperature distribution is applied: within the urban pattern as shown in Figure 4, a Gaussian profile with a peak value of $\vartheta_{hot} = 0.5$ is prescribed, whereas a constant temperature is imposed outside this region. The maximum temperature difference across the fluid layer is thus defined as $\Delta = \vartheta_{hot} - \vartheta_{bottom} = 1$.

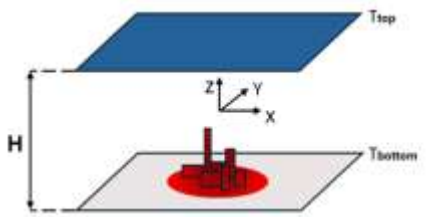

$$T_{top} = T_{atmosphere} \leq T_{country} \leq T_{city}$$

Figure 3. Schematic representation of the computational domain and boundary conditions

Figure 4. Skyline of the created city pattern

The simulation parameters are summarized in Table 2.

After an initial transient, velocity, pressure and temperature fields are collected when the system reaches a statistically steady state characterized by an average Nusselt number of Nu = 15 computed at the top plate, and with a time interval larger than the time eddy turnover given by $T_{free\ fall} = H/U_{ff}$.

Table 2. Simulation parameters

(Lx, Ly, Lz)	(nx, ny, nz)	$\Delta\tau$	T
$(8R, 8R, 1.05R)$	(1600,1600,263)	2.6	354

Notes: $\Delta\tau$ is the time interval between consecutive fields used for statistical averaging; T is the total simulation time

Recalling the final set of parameters used for the city generation, as reported in Table 1, we can identify a non-dimensional roughness thickness k_z^*, given by the ratio between the thermal boundary layer thickness $\delta_t = H/(2Nu)$, and the mean buildings height, that provides a measure of how strongly the urban geometry interacts with the thermal boundary layer. In our case, we find $k_z^* \sim 0.88$.

4. FLOW TOPOLOGY

The statistical symmetries of the flow solution are better expressed in a cylindrical coordinate system $(r, \theta, z) \in [0, 4] \times [0, 2\pi] \times [0, 1]$.

Furthermore, due to the presence of the city within the domain, the statistics have been subdivided into two main regions to allow for a more detailed analysis: a lower region defined by $z \in [0,0.2]$ and an upper region defined by $z \in [0.2,1]$.

To maintain a coherent visualization across variables, all contour plots use the same colour scale range and fixed shell spacing.

Mean quantities have been computed by considering homogeneity in the azimuthal direction, over concentric cylindrical shells with a radial thickness of $16\Delta x = 0.08$ reference length. Temporal averaging was also performed over 56 distinct time instants to ensure statistical convergence.

4.1 Mean quantity contour

Looking at the upper region, by analyzing the contours of mean radial statistics in r-z plane, as Figure 5, for the temperature field and Figure 6, for the vertical velocity, it is possible to note a small region above the city pattern characterized by higher temperature contrast compared to the surroundings and with a positive mean vertical velocity. This indicates the presence of an upward plume rising from the city roughness. Once the plume reaches the top boundary, the imposed free slip boundary conditions on the velocity fields results in a positive radial velocity, as it is shown in Figure 7, directed from the center of the top plate towards its edge.

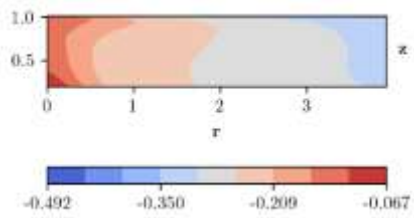

Figure 5. Time-average temperature $\langle\vartheta\rangle$

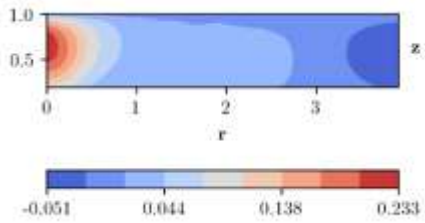

Figure 1. Time-averaged vertical velocity $\langle W\rangle$

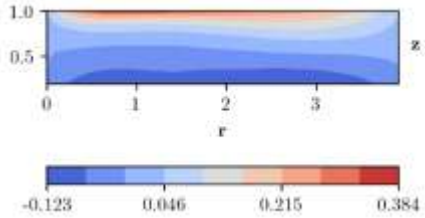

Figure 2. Time-averaged radial velocity $\langle Ur\rangle$

Even though statistics are only computed from $z = 0.2$, up to the top boundary, the contour reveals the presence of a mean circular wind pattern or large scale circulation, that develops above the city pattern, intensifies up to the top boundary, then spreads radially outward toward the edge of the domain, descends along the outer region and returns towards the urban area.

This overall dynamic is clearly illustrated in Figure 8, which shows a zoomed-in snapshot size $(Lx, Ly, Lz) = (2,2,1)$, from the simulation. In this figure, buildings are represented using the zero level-set of the signed distance field, coloured by temperature field. A temperature contour $\vartheta = -0.1$ highlights a hot flow column originating from the urban area, rising through the domain, and extending toward the top boundary, supporting the description of the plume and the associated circulation.

Figure 8. Zoomed-in snapshot showing the temperature field contour at $\vartheta = -0.1$ over the urban area, contour of the signed distance field, at $\Phi = 0$, coloured by temperature

5. CONCLUSIONS

UHI is one of the most widely studied phenomena in urban climatology over the past decades. In this study, we have developed a general framework to represent a variety of idealized urban patterns using only five parameters. These parameters capture key morphological characteristics, such as coverage density, mean height, and spatial distribution, that are measurable from real urban layouts.

For the first time, a Direct Numerical Simulation of such an idealized configuration has been performed, consisting of 176 buildings, with the aim of exploring the fundamental mechanisms governing heat transfer under buoyancy-driven flow conditions. The proposed setup provides a highly controlled and repeatable environment to isolate the influence of urban morphology on thermal processes.

While many other studies focus on specific neighborhoods, the present work adopts an idealized and general approach for an entire city pattern. This generalization allows for a more fundamental understanding of the physical mechanism, free from the geometric and contextual constraints of a specific urban case.

Findings obtained through this approach can be generalized and subsequently applied to more realistic and site-specific configurations

Future developments of this work may include the introduction of a mean wind to assess the combined effect of shear and buoyancy driven flows. Additionally, the influence of both physical parameters, such as k_z^* and morphological features of the city could be systematically varied to better understand the dominant mechanisms that control thermal exchanges and to identify effective strategies for urban climate mitigation. Moreover, given the high computational cost of DNS, future investigations could benefit from the use of Large Eddy Simulations (LES) to explore a wider range of configurations within reasonable time frames and, above all, reduce the time costs.

In summary, this study provides a novel and flexible approach that can serve as a reference for future numerical investigations on UHIs.

ACKNOWLEDGMENT

We wish to acknowledge the Italian supercomputing center CINECA that under the ISCRA B project FGWW provide the HPC resources for the simulations as well as Delft High Performance Computing Centre (DHPC) through the DelftBlue Supercomputer (Phase 2), 2024.

This work is supported by the National Recovery and Resilience Plan, NRRP (Grant No.: 00010502).

REFERENCES

[1] Masson, V., Heldens, W., Bocher, E., Bonhomme, M., et al. (2020). City-descriptive input data for urban climate models: Model requirements, data sources and challenges. Urban Climate, 31: 100536. https://doi.org/10.1016/j.uclim.2019.100536

[2] Masson, V., Lemonsu, A., Hidalgo, J., Voogt, J. (2020). Urban climates and climate change. Annual Review of Environment and Resources, 45(1): 411-444. https://doi.org/10.1146/annurev-environ-012320-083623

[3] Oke, T.R., Mills, G., Christen, A., Voogt, J.A. (2017). Urban Climates. Cambridge University Press.

[4] Howard, L. (1818). The Climate of London. (London: W Phillips, sold also by J and A Arch).

[5] Assenova, I.A., Vitanova, L.L., Petrova-Antonova, D. (2024). Urban heat islands from multiple perspectives: Trends across disciplines and interrelationships. Urban Climate, 56: 102075. https://doi.org/10.1016/j.uclim.2024.102075

[6] Kabisch, N., Remahne, F., Ilsemann, C., Fricke, L. (2023). The urban heat island under extreme heat conditions: A case study of Hannover, Germany. Scientific Reports, 13(1): 23017. https://doi.org/10.1038/s41598-023-49058-5

[7] Kotharkar, R., Ramesh, A., Bagade, A. (2018). Urban heat island studies in South Asia: A critical review. Urban Climate, 24: 1011-1026. https://doi.org/10.1016/j.uclim.2017.12.006

[8] Barlow, J., Coceal, O. (2008). A review of urban roughness sublayer turbulence. Technical Report, University of Reading.

[9] Sutzl, B.S. (2021). Rising from the ground: Distributed drag parameterization of urban environments for numerical weather prediction. Doctoral Dissertation, Imperial College London.

[10] Chen, B., Wang, W., Dai, W., Chang, M., et al. (2021). Refined urban canopy parameters and their impacts on simulation of urbanization-induced climate change. Urban Climate, 37: 100847. https://doi.org/10.1016/j.uclim.2021.100847

[11] Rostami, E., Nasrollahi, N., Khodakarami, J. (2024). A comprehensive study of how urban morphological parameters impact the solar potential, energy consumption and daylight autonomy in canyons and buildings. Energy and Buildings, 305: 113904.

https://doi.org/10.1016/j.enbuild.2024.113904
[12] Neophytou, M. (2005). Modelling the wind flow in complex urban topographies: A Computational-Fluid-Dynamics simulation of the central London area. In Proceedings of the 5th GRACM Inter Congress on Comput Mech, Limassol, Cyprus, pp. 967-974.
[13] Chen, H., Zhu, S., Ye, T., Miao, Y. (2025). Optimizing urban ventilation in heritage settings: A computational fluid dynamics and field study in Zhao'an Old Town, Fujian. Buildings, 15(3): 483. https://doi.org/10.3390/buildings15030483
[14] Giometto, M.G., Christen, A., Meneveau, C., Fang, J., Krafczyk, M., Parlange, M.B. (2016). Spatial characteristics of roughness sublayer mean flow and turbulence over a realistic urban surface. Boundary-Layer Meteorology, 160(3): 425-452. https://doi.org/10.1007/s10546-016-0157-6
[15] Hertwig, D., Efthimiou, G.C., Bartzis, J.G., Leitl, B. (2012). CFD-RANS model validation of turbulent flow in a semi-idealized urban canopy. Journal of Wind Engineering and Industrial Aerodynamics, 111: 61-72. https://doi.org/10.1016/j.jweia.2012.09.003
[16] Ricci, A., Kalkman, I., Blocken, B., Burlando, M., Freda, A., Repetto, M.P. (2017). Local-scale forcing effects on wind flows in an urban environment: Impact of geometrical simplifications. Journal of Wind Engineering and Industrial Aerodynamics, 170: 238-255. https://doi.org/10.1016/j.jweia.2017.08.001
[17] Xie, Z., Castro, I.P. (2006). LES and RANS for turbulent flow over arrays of wall-mounted obstacles. Flow, Turbulence and Combustion, 76(3): 291-312. https://doi.org/10.1007/s10494-006-9018-6
[18] Ricciardelli, F., Polimeno, S. (2006). Some characteristics of the wind flow in the lower Urban Boundary Layer. Journal of Wind Engineering and Industrial Aerodynamics, 94(11): 815-832. https://doi.org/10.1016/j.jweia.2006.06.003
[19] Zaki, S.A., H'ng, Y.M., Mohammad, A.F., Ardila-Rey, J.A., Alam, N., Ahmad, M.I. (2025). Vertical wind profile distribution within canopy layer based on representative geometry model using wind tunnel experiment. Scientific Reports, 15(1): 1117. https://doi.org/10.1038/s41598-024-83400-9
[20] Castro, I.P., Xie, Z.T., Fuka, V., Robins, A.G., et al. (2017). Measurements and computations of flow in an urban street system. Boundary-Layer Meteorology, 162(2): 207-230. https://doi.org/10.1007/s10546-016-0200-7
[21] Gray, D.D., Giorgini, A. (1976). The validity of the Boussinesq approximation for liquids and gases. International Journal of Heat and Mass Transfer, 19(5): 545-551. https://doi.org/10.1016/0017-9310(76)90168-X
[22] Costa, P. (2018). A FFT-based finite-difference solver for massively-parallel direct numerical simulations of turbulent flows. Computers & Mathematics with Applications, 76(8): 1853-1862. https://doi.org/10.1016/j.camwa.2018.07.034
[23] Yang, J., Balaras, E. (2006). An embedded-boundary formulation for large-eddy simulation of turbulent flows interacting with moving boundaries. Journal of Computational Physics, 215(1): 12-40. https://doi.org/10.1016/j.jcp.2005.10.035

NOMENCLATURE

A_π	average building planform area
A_{tot}	total plan area of all buildings
AR_π	average planform aspect ratio
AR_z	average city vertical aspect ratio
AR_{zcity}	reference aspect ratio of building heights
$\Delta\vartheta$	temperature difference between top plate and city center
Δt	time interval between collected fields
Δx	grid spacing x direction
δ_t	thermal boundary layer thickness
f_{random}^n	generator functions of random modifiers for geometry generation
$g(r)$	radial smoothing function
H	cell heigth
k_z^*,	dimensionless roughness thickness
L_x, L_y, L_z	domain length in x,y,z directions
l_x	average shorter planform length
l_y	average longer planform length
l_z	average building vertical length
l_{free}	free space between buildings
l_{free}^{ref}	reference free space
n	total number of buildings
n_x, n_y, n_z	number of grid points in x,y,z directions
Nu	Nusselt number
p	pressure
Pr	Prandtl number
R	city radius
Ra	Rayleigh number
r	radial coordinate in cylindrical system
ρ	average density coverage, dimensionless
T	total simulation time
$T_{free\ fall}$	free fall time scale
U_{ff}	free fall velocity
u_i	velocity component (i=1,2,3)
x_1, x_2	x-coordinates of the first vertex of two consecutive buildings
y_1, y_2	y-coordinates of the first vertex of two consecutive buildings
z	vertical coordinate in cylindrical system

Greek symbols

ϑ_{hot}	maximum temperature at the top plate
ϑ_{bottom}	background temperature outside urban area
ϑ_{cold}	temperature at the top plate
Θ	temperature field
α	thermal diffusivity
β	thermal expansion coefficient
Φ	signed distance field
γ	orientation angle of building
ε	coefficient describing radial variation of city shape
λ	average coverage frequency
θ	azimuthal coordinate in cylindrical system
υ	kinematic diffusivity

Subscripts

city	computed at city
ff	refers to free-fall characteristic scale

free	free separation
i,j	spatial indices
random	stochastic variation
t	refers to thermal
tot	total
x,y,z	spatial directions
π	planform related quantity

Superscripts

ref	reference value